Ph.D. Thesis

Tissue Classification of Atherosclerotic Coronary Plaque from Imbalanced IVUS Data Sets Using Deep Boltzmann Machine

(ディープ・ボルツマン・マシンを使ったデータ数が不均衡なIVUSデータからの動脈硬化冠動脈プラークの組織分類)

2018

ぐえん　ちょん　くおん

NGUYEN TRONG KUONG

Advisor: Prof. Eiji Uchino

Graduate School of Science and Engineering
Yamaguchi University

Acknowledgment

I am so grateful to the individuals who have given me precious time and invaluable guidance throughout the study. First of all, I would like to express my sincere thanks to my advisor, Prof. Eiji Uchino who has been always enthusiastic to read and reread my writings, and given me precious discussions. Also, many thanks to the friends who directly discussed with me about the research in the laboratory.

I very much appreciated the financial support of the Vietnam International Education Cooperation Department (VIED) and the MOU signed between the VIED and Yamaguchi University in pursuing my graduate study.

Special thanks to my family, they have always been encouraging me and filled with more respect and higher expectations for my profession than I have ever had.

Abstract

This dissertation presents a study of tissue characterization of human atherosclerotic coronary plaque by deep Boltzmann machine (DBM). The research data sets include intravascular ultrasound (IVUS) radiofrequency signals acquired from human coronary arteries. IVUS tissue characterization has been an issue of great concern in medical application studies for the reason that coronary heart disease (CHD) statistically accounts for a high proportion of mortality whereas the formation of atherosclerotic plaque is a leading cause of CHD.

In machine learning, deep networks have attracted much interest in recent years, which play as powerful frameworks to handle with large and high dimensional data sets. Restricted Boltzmann machine (RBM) is a good initialization for constructing deep networks. In addition, RBM is developed as a stand-alone classification network for supervised learning, so it has attracted many studies recently. The aim of this thesis is to provide insights into learning features of imbalanced IVUS data sets to classify IVUS tissues by the use of RBM and DBM.

Structurally, this dissertation is organized in seven chapters. The two first chapters introduce about our IVUS data sets and the interested classifiers. The next chapters present the results of tissue classification with respect to specific methods. The details of each chapters are summarized as follows:

Chapter 1 describes the IVUS data sets and our target problem of IVUS tissue classification. Related work and background in the literature of IVUS tissue characterization are briefly reviewed. In particular, a brief description of how to acquire IVUS signals, concerned techniques of IVUS signal preprocessing are presented. Besides that, the literature of imbalanced dataset learning is analyzed in relation to our present topic, specially, the evaluation for multiclass classification and the difficulties of class imbalance problem.

Chapter 2 describes the network structure of RBM. Its capacity for unsupervised learning and learning stability are discussed. Regarding supervised learning, RBM is developed as a stand alone classification model, it is called classification restricted Boltzmann machine (ClassRBM). Next, deep Boltzmann machine (DBM) is presented as an interested deep network.

With a step-by-step approach, our first results in this dissertation are mainly from using ClassRBM. After dealing the difficulties of class imbalances and understanding the learning capacity of ClassRBM, the deep network DBM is a next consideration in order to improve tissue classification performance.

Chapter 3 presents the IVUS tissue classification by ClassRBM in comparison to integrated backscatter method (IB-IVUS) which is as a conventional method in the literature of IVUS tissue characterization. The results show a better classification evaluation performed by ClassRBM as compared to IB-IVUS for the same task. Above all, this study shows a more understanding of ClassRBM when featured IVUS patterns are proposedly binarized. That work proves an advantage as compared to the classification of ClassRBM performed with real-valued featured patterns, hence the bit level of IVUS data is a considerable point regarding the use of ClassRBM.

Chapter 4 shows efforts to deal with the class imbalances of IVUS data sets that hinder the training of RBM. Balancing training sets is first concerned by the use of adaptive synthetic sampling technique (ADASYN) which employs oversampling, undersampling and synthetic sample creating to balance training sets. Another consideration is the use of multiclass AdaBoost which ensembles ClassRBMs. This chapter mainly focuses on the frequency domain of IVUS signals. The tissue class imbalances are still obstacles and challenges for training of ClassRBM although the results show little improvement of tissue classification by comparison of ClassRBM with neural networks and support vector machine.

Chapter 5 takes pixel level of dataset into account and presents a proposed training algorithm of ClassRBM with a misclassification cost-sensitive algorithm to address IVUS dataset imbalances. In words, the proposed algorithm is a strategy to accumulate training sets step-by-step which is based on the misclassification rate of each class. The proposed misclassification cost-sensitive algorithm supports the training of ClassRBM better as compared to neural network for the same network size and same task.

Chapter 6 shows an application of deep Boltzmann machine with the understandings from previous chapters. Particularly, the misclassification cost-sensitive training algorithm in chapter 5 is simplified. In addition, using unsupervised learning is first considered and fed for supervised learning in the upper layer of DBM. In other words, DBM contains stacked RBMs of which the first RBM squeezes input data and feeds for the upper one where the uppermost layer is ClassRBM. DBM proves a high representation for the tissue classification. The results also show the better performance by DBM as compared to IB-IVUS. In addition, in this chapter, different sizes of IVUS patterns are paid attention to specify a better size in IVUS pattern extraction.

Chapter 7 is for our conclusion, the achieved results are promising to encourage us to improve the IVUS issue towards the application of deep learning. The limitations of our method are inevitable points discussed here for future work.

In sum, in attempting to improve the IVUS tissue classification, this dissertation shows a step-by-step approach to deal with the obstacles of IVUS data sets as well as the network derived from restricted Boltzmann machines. In a nutshell, the data binarization and misclassification cost-sensitive training algorithms of ClassRBM and DBM are the key solutions to solve the IVUS tissue classification issue.

Contents

List of Figures

List of Tables

List of Algorithms

Chapter 1

Introduction

1.1 Coronary atherosclerosis and IVUS method

Cardiovascular diseases such as heart attack or stroke account for high rates of mortality [1]. Coronary atherosclerosis, a disease of coronary artery wall, is the major cause of cardiovascular diseases. It is diagnosed on the detection of atherosclerotic plaque inside coronary arteries. Atherosclerotic plaque is the major risk factor for heart failure because it narrows the arteries when coronary plaque develops, and in final stage plaque rupture occurs that causes a blood block.

Many research efforts have been devoted to understanding atherosclerotic plaque morphology and rupture-proneness [2, 3]. The presence of fibrous cap encaging a central lipid core is the predicted precursor of plaque rupture. Early detection of vulnerable plaques in vivo is essential to assess their progress and to evaluate potential treatment modalities which may ultimately impact on the prevention of heart failure. A particular example from the data sets of this study is shown in Fig. 1.1, the vessel section stays at the left anterior descending (LAD) coronary artery of a patient. According to the examinations, medical expert identified atherosclerotic plaque containing fibrofatty, fibrocellular, fibroacellular and lipid.

Intravascular ultrasound (IVUS) is a medical imaging methodology using a designed ultrasound transducer probe which allows the state observation of the vessel wall and lumen, monitoring and quantifying its compositions. The acquired ultrasound signals are then processed by a computerized program to visualize the intra vessel. Fig. 1.2 illustrates the process from the ultrasound observation by a transducer to the B-mode image screened by a computerized program. When the transducer probe is located at a target position of vessel as in Fig. 1.2(a), it emits ultrasound beams to tissues and

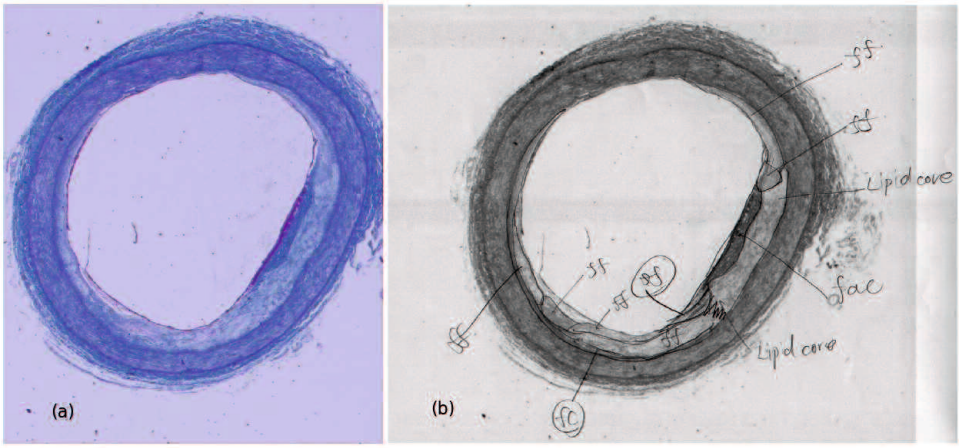

Figure 1.1: Plaque component identification, (a) is the stained film of coronary section, (b) shows delineated components of (a) drawn by the medical experts including fibrofatty (ff), fibroacellular (fac), fibrocellular (fc) and lipid core.

senses the backscattered signals. In addition, due to the rotation ability of the transducer, different directions of vessel cross sectional plane are investigated corresponding to A-lines as plotted in Fig. 1.2(b). Thanks to Hilbert transform [4], amplitude envelopes of the whole signals of cross section are extracted and transformed into gray scale in order to visualize the cross sectional plane of the vessel at the probing point, this shows as the first use of

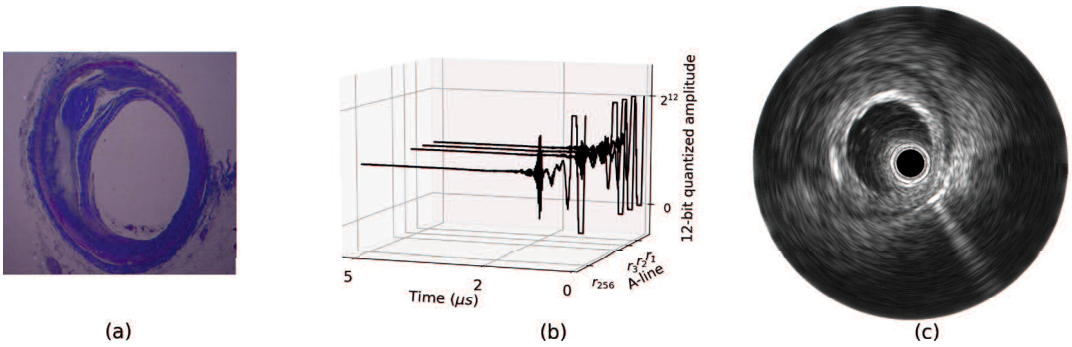

Figure 1.2: Ultrasound acquisition and B-mode image construction of vessel cross section. IVUS transducer probe reaches at a given section as picture (a) and carries out ultrasound observation, 256 backscattered signals corresponding to 256 different angles are collected in picture (b), and picture (c) is the B-mode image constructed from the acquired signals.

the acquired signals. It is called B-mode image as seen in Fig. 1.2(c).

Yet, the IVUS signals have not shown immediately the properties associated with tissue components, and neither has B-mode image displayed tissues explicitly. Thus, it needs an intermediate process to find out the characteristics of tissues in relation to their backscattered amplitudes. This is illustrated from the comparison and contrast between the true vessel section, its B-mode display and the plaque area identified by medical experts as in Fig. 1.3. Here, to display the region of interest (ROI) as Fig. 1.3(c), the medical experts identified tissues from the stained slice film (Fig. 1.3(a)) and morphed corresponding plaque area into its B-mode image (Fig. 1.3(b)).

In short, there are two main processes of IVUS methodology which include data acquisition and data analysis. While data acquisition depends on the IVUS device and the examination conduction, in the next step after data acquisition, how well tissues are characterized, it depends on the data analysis model used.

1.2 IVUS research data sets

The IVUS data sets for our study are from the graduate school of medicine, Yamaguchi University. We have full approval of ethics committee for study. The data sets include coronary vessels of human left anterior descending (LAD) and left circumflex coronary arteries (LCX). They were acquired under the examinations conducted by medical experts in the graduate school

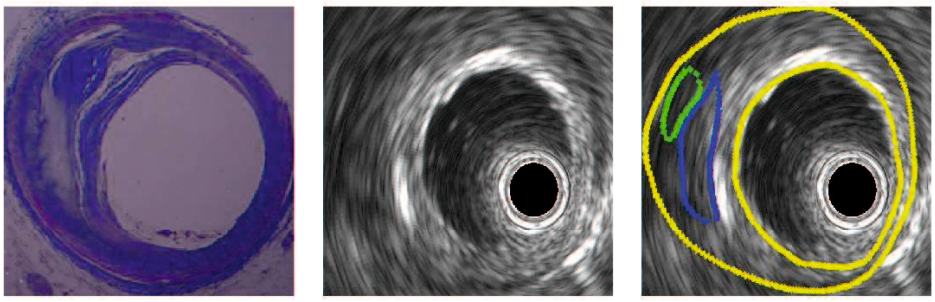

Figure 1.3: Plaque component identification by medical experts, (a) is stained film image, (b) is B-mode image, and (c) shows plaque areas morphed corresponding between (a) and (b) where fibrofatty is drawn by green line, fatty is drawn by blue line, and the rest area between yellow lines is fibrous.

of medicine.

In those examinations, Galaxy IVUS imaging device (Boston Scientific, USA) with a 40 MHz transducer was used for the ultrasonic observation. The transducer rotation was 30 revs/s, sampling rates of 210 and 400 MHz and 256 signal lines were collected per one revolution.

Immediately after the ultrasonic observation, the coronary sections were stained with Masson's Trichrome method. Then, plaque was manually delineated by medical experts from the stained film observations. To clarify the rotational position of the sections which would be observed, stainless steel needles were carefully inserted into those sections in advance to be used as a reference point to track the corresponding IVUS frame.

1.3 IVUS signal characterization problem

As presented in section 1.1, acquired IVUS signals need to be carefully analyzed by a data analysis model to characterize how plaque tissues react to ultrasound. Theoretically, IVUS radiofrequencies contain informative measures of intrinsic plaque features. In experimental reality, however, IVUS acquisition and informative feature extraction are very complicated. Katouzian et al. [5] shows challenges from data acquisition to classification of this method while the reliability of training dataset and the complexility of recognition algorithm can highly impact the accuracy of characterization. The following subsections present the problems involving IVUS tissue characterization we are interested in.

1.3.1 Noise removal

Just after IVUS signal acquisition, the immediate problem is to process noise of IVUS signals. Due to noise, it challenges any classification models not only in IVUS characterization but also in other research fields of signal processing. Noise is often unknown. Various artifacts affect the data collection, thus handling noise is laborous. In particular, some advanced studies [6, 7] investigate noise acted by blood flow. When noise is blind, statistical methods which are fundamental tools are used to evaluate noise. In this study, we consider outliers defined by statistical techniques are noise and remove them for the next analysis.

1.3.2 Data standardization

Data standardization is essential to avoid incompatible data in IVUS classification problems [8–10]. It includes the standardization of data for classification and for evaluation methodology. In IVUS data preprocessing, there are some common steps [10] as listed in the follows we use them in the study.

Time gain compensation (TGC). This procedure aims to compensate the attenuation of ultrasound signals due to depth. That is done by the following attenuation function:

$$T(r) = 1 - e^{-\beta r}, \tag{1.1}$$

where $\beta = \log 10^{0.18*f/20}$, f is the frequency of the transducer (MHz), r is the radial distance from catheter (cm).

Data normalization. To homogenize the data sets in the same range, there are some norms used to transform data into unit interval. Specifically, Eq. (1.2) shows the data normalization by minmax norm which is often used in our study.

$$R_{norm} = \frac{R - R_{\min}}{R_{\max} - R_{\min}}. \tag{1.2}$$

1.3.3 Signal representation domain

Ultrasonic waves are real-time continuous but the acquired signals sensed by IVUS device are sampled at a specific sampling rate. Time-series domain allows to locate radiofrequency amplitudes of signal corresponding to their distance when sound speed is specified in advance. Frequency is another fundamental domain in signal processing. These two kinds of signal representation have a tight relationship by Fourier transform.

Theoretically, the relationship between time series and frequency is defined by time-frequency transform [11] as Eq. (1.3), where t, ω are time and frequency variables, $h(t)$ is a window function.

$$S_t(\omega) = \frac{1}{2\pi} \int e^{-j\omega\tau} s(\tau) h(\tau - t) d\tau. \tag{1.3}$$

Feature extraction depends on a specific problem and the data representation domain the researchers are interested in for analysis.

1.3.4 Multiclass classification evaluation

Multiclass classification problem means that the number of classes are more than two. For the case of two classes, it is called binary classification. The performance of classification is evaluated based on the quantitative measures which are calculated from the analysis between true sets and predicted sets. Evaluation measures play a crucial role in classifier design to evaluate the performance of a learning paradigm. In many cases, evaluation measures for the multiclass problems are developed from the binary ones. Sometimes, they are well understood in binary cases but perform poor in multiclass cases.

More specifically, let us consider the binary classification first. Table 1.1 shows the confusion matrix of binary classification with two classes A_1 and A_2. Refer to this matrix, the most common used measure in classification is overall accuracy which is calculated as Eq. (1.4).

$$Overall\ accuracy = \frac{\sum_{i=1}^{2} n_{ii}}{\sum_{i,j=1}^{2} n_{ij}}. \tag{1.4}$$

Regarding individual evaluation, two measures *recall* and *precision* are considered [12]. Specifically, let R_i and P_i denote *recall* and *precision* of class A_i, $i = \{1, 2\}$, respectively. Then, they are defined as:

$$R_i = \frac{n_{ii}}{n_{i1} + n_{i2}}, \tag{1.5}$$

$$P_i = \frac{n_{ii}}{n_{j1} + n_{j2}}. \tag{1.6}$$

Recall shows that on a given class set how many percent of correct samples the classifier identified. While *precision* reflects the ability of recognizing relevent samples. In other words, *precision* shows that among the samples predicted as the same class how many percent of accurately predicted samples are. Lewis et al.[13] suggested *F-measure*[14] which integrates these two measures as the following equation:

$$F - measure_i = \frac{2R_iP_i}{R_i + P_i}. \tag{1.7}$$

Table 1.1: Confusion Matrix of Classification

		Predicted class	
		A_1	A_2
True class	A_1	n_{11}	n_{12}
	A_2	n_{21}	n_{22}

Alternatively, these measures are developed in the extension to k classes ($k > 2$). However, there are two considerable approaches: one-versus-one and one-versus-all [15–17]. In words, each individual class is evaluated in pairs with one another or against with all others. The first case requires a class pair decomposition. As a result, there have been more indexes for decision, it leads to a problem of multi decision making. Clearly, the more measures used the more difficulties in making decision. In common, learning models prefer overall performance evaluation such as overall accuracy. Besides overall accuracy, another such overal evaluation measures are G-mean [18] which is defined as Eq. (1.8) and MAUC [19] which stands for multiclass area under curve. They are used to interpret some our results.

$$G\text{-}mean = \sqrt[k]{\prod_i R_i}. \tag{1.8}$$

1.3.5 Class imbalance problem

In many real world applications, it is usually faced to the problem of imbalanced data sets [20]. Imbalanced data sets mean one class outrepresents the others, the distribution between classes is significantly different. For instance, the proportion of two classes is 1:100, 1:1000, etc. Since almost all traditional classifiers seek the overall accuracy more than individual, the classification evaluation needs careful considerations, even some evaluation indexes become invaluable. For example, let us consider the binary classification problem where the ratio of the number of two classes is 1:100, if a classifier identifies all elements as the major class, the achieved overall accuracy is 99%. It seems too good but that classifier is biased towards the major set and not worthy if the objective is to recognize minor class. Usually, such problems have multiple classes with different proportions and the rare classes are targeted objects of research.

Up to now, class imbalance tasks are faced to two main difficulties: (i) how to deal with class imbalances, and (ii) how to evaluate the prediction. Nonetheless, the way to interpret the result is important, and another difficulty is how to train a classifier to handle both major and minor classes. At dataset level, there have been a number of techniques to rebalance the training data sets, they can be roughly categorized into (i) oversampling by creating more synthetic samples of minor class, and (ii) undersampling by removing a number of samples of major sets. These cases have been concerned in many recent studies [20–24]. Another solution to deal with class imbalances studied is bootstrapped sampling as in [25–27].

An another solution to deal with imbalanced datasets is to integrate learn-

ing models, it is catgorized in the group of ensemble methods. For example, AdaBoost [28], random forest [29]. Each such classifier may incorporate a specific technique of sampling. For example, removing instances of major sets which are far from borderlines can boost the training of support vector machine as studied in [30], or using cost function to select the number of training for neural network as in [22].

Chapter 2

Deep Boltzmann Machine

This chapter first introduces about restricted Boltzmann machine (RBM), its capacity to extract features from input data for unsupervised learning. Then, for the classification task, two supervised learning settings of RBM are presented. Finally, deep Boltzmann machine which is constructed by RBMs is presented.

2.1 Restricted Boltzmann machine

Restricted Boltzmann machine (RBM) [31] is a probabilistic network that employs binary hidden variables $h = (h_1, \ldots, h_H)$ to learn the distribution of visible variables $x = (x_1, \ldots, x_N)$. Each visible unit x_i has an undirected connection W_{ij} to each hidden unit h_j. There is no connection between the same class units. Values $b_i's$ and $h_j's$ are biases for input units x and hidden units h. Fig. 2.1 shows the network structure of RBM including visible layer x and hidden layer h, W stands for connection weights between these two layers. The behaviors of the network will be observed under the change of the energy function defined by:

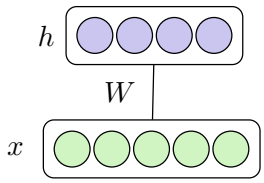

Figure 2.1: Graphical representation of restricted Boltzmann machine.

$$E(x,h) = -\sum_{i,j} W_{ij} x_i h_j - \sum_i b_i x_i - \sum_j c_j h_j \,. \tag{2.1}$$

The joint distribution $P(x,h)$ is defined by:

$$P(x,h) = \frac{exp(-E(x,h))}{Z}\,, \tag{2.2}$$

where Z is a normalization constant. The conditional probabilities for visible units and hidden units are:

$$P(h_j \mid x) = sigm(\sum_i W_{ij} x_i + c_j) \tag{2.3}$$

and

$$P(x_i \mid h) = sigm(\sum_j W_{ij} h_j + b_i)\,, \tag{2.4}$$

where $sigm(x) = \dfrac{1}{1+e^{-x}}$ is a sigmoid function. The RBM model is briefly illustrated in Fig. 2.1.

With contrastive divergence algorithm (CD) [32, 33], RBM has demonstrated its capacity to be a powerful model to extract features from high dimension dataset for the unsupervised learning problems, or it is used to build deep artificial neural networks. Particularly, CD algorithm seeks the generative distribution of input and hidden units, thus hidden units become as intermediate units to understand input data. Alternatively, hidden units can be fed for deeper networks. RBM is a good initialization for constructing deep network to handle big data [34], that explains why RBM has attracted much attention recently.

The above network is set up with binary data inputs, it is called Bernoulli RBM. Gaussian RBM [32] is an another version associating to real-valued inputs. To control the sparsity of input data, regularization is used, for example, Ngiam et al.[35] proposed a penalty to regularize RBM model for sparsity. In our studies, we often use L_2-regularization for sparsity [36].

In addition, RBM can be developed as a standalone classifier. The following section will present an implementation of RBM to tackle the classification problem.

2.2 Classification restricted Boltzmann machine

As above mentioned, restricted Boltzmann machine has been interested in a variety of learning problems [31]. It plays as an unsupervised learning model,

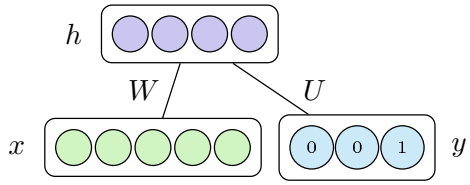

Figure 2.2: Graphical representation of ClassRBM which shows hidden layer h, input layer x and its class y. W and U are connections between hidden units and class units, respectively.

and as an initializiation for deep belief networks [34]. However, this network is also developed as a self-contained framework for classification, it called classification restricted Boltzmann machine (ClassRBM) [37].

Firstly, let have a look at the network stucture of ClassRBM as in Figure 2.2. Structurally, ClassRBM is an extension of standard restricted Boltzmann machine (RBM) by adding binary class units that encode the label of the data input. In words, if input vector x has class label k, then the corresponding class vector is $y_k = (0, \ldots, \overset{(k)}{1}, \ldots) \in \{0,1\}^K$. Here, K is the number of classes of data set and also the number of class units of ClassRBM network. The energy function is defined by Eq. (2.5).

$$\begin{aligned} E(x,h,y_k) = &-\sum_{i,j} W_{ij}x_ih_j - \sum_i b_ix_i - \sum_j c_jh_j \\ &- \sum_j U_{kj}h_j - d_k, \end{aligned} \tag{2.5}$$

where U_{kj} and d_k are connection weights, and biases in relation to the class unit k. There is no connection between visible units and class units. The energy function defines the following joint distribution:

$$P(x,h,y) = \frac{exp(-E(x,h,y))}{Z}, \tag{2.6}$$

where Z is a normalizing constant, and the conditional probabilities are defined:

$$P(h_j \mid x, y_k) = sigm(\sum_i W_{ij}x_i + U_{kj} + c_j) \tag{2.7}$$

and

$$P(x_i \mid h) = sigm(\sum_j W_{ij}h_j + b_i)\,, \tag{2.8}$$

$$P(y_k \mid h) = \frac{exp(\sum_j U_{kj} h_j + d_k)}{\sum_l exp(\sum_j U_{lj} h_j + d_l)} \,. \tag{2.9}$$

The posterior probability for classification is:

$$P(y_k \mid x) = \frac{exp\Big(d_k + \sum_j f(\sum_i W_{ij} x_i + U_{kj} + c_j)\Big)}{\sum_{y_l} exp\Big(d_l + \sum_j f(\sum_i W_{ij} x_i + U_{lj} + c_j)\Big)} \,, \tag{2.10}$$

where $f(x) = \log(1 + exp(x))$ is the softplus function.

In terms of training algorithms of ClassRBM, Larochelle et al.[37] showed two possible learning cases of ClassRBM corresponding to two kinds of learning objective functions to be optimized as the follwings.

Generative learning (GenRBM). This model aims to optimize the joint distribution of input and label data. Specifically,

$$\log P(x_t, y_t) \longrightarrow \quad \max.$$

Discriminative learning (DisRBM). This model aims to maximize the discriminative probability of class given input data. Specifically,

$$\log P(x_t |\, y_t) \longrightarrow \quad \max.$$

However, using generative training or discriminative training depends on how misspecified the model is, and the hybrid case is also considered [37]. In case of real-valued input data with the assumption of Gaussian distribution [31], visible variable x_i varies around the mean b_i and its standard deviation σ_i. The energy function is replaced by:

$$\begin{aligned} E(x, h, y_k) = & \sum_i \frac{(x_i - b_i)^2}{2\sigma_i} - \sum_{i,j} \frac{x_i}{\sigma_i} W_{ij} h_j \\ & - \sum_j c_j h_j - \sum_j U_{kj} h_j - d_k. \end{aligned} \tag{2.11}$$

Obvisously, for the two abovementioned training modes which one is chosen it depends on the training target. A very careful discussion about the training stability in relation to these modes is presented in [31].

2.3 Deep Boltzmann machine

In the above subsections, the supervised and unsupervised learning model of RBM are introduced. In supervised learning, a class layer is added to incorporate the classification model of RBM. For the unsupervised learning, RBM hidden layer encodes the input layer of RBM. Fig. 2.3 shows a DBM network with an input layer and hidden layers. Architecturally, DBM includes stacked hidden layers where the precedent hidden layer will pay as the input layer of the succeeding RBM.

Deep networks has attracted enthusiastic interest in recent years. The studies [38, 39] show the powerful effect of those models to solve learning problems with big data. DBM is architected by stacking RBMs, algorithms of training RBM are employed to train DBM. Often, DBM is trained greedy layer-wisely and then cost function defined by log likelihood or cross entropy loss is minimized log-likelihood [32, 34, 35, 39].

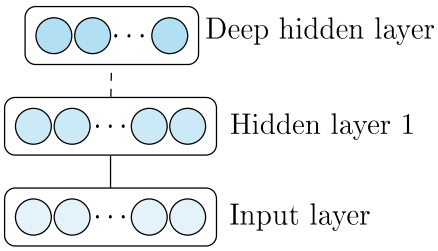

Figure 2.3: Network structure of deep Boltzmann machine.

Chapter 3

Data Binarization for Restricted Boltzmann Machine

This chapter introduces a study of IVUS data binarization for ClassRBM. The results are presented in [40].

3.1 Background

Frequency analysis method is widely used for IVUS signal processing. In particular, integrated backscattered IVUS or IB-IVUS [41] is as a conventional method which analyzes the ultrasound backscattered power to identify the difference of acoustic characteristic impedance that is determined by the density of tissue. However, the tissue characteristics are uneasily determined by the domination of various factors and by the robustness of data. The studies in [3, 5] showed the complexity of atherosclerotic plaque characterization, which requires a careful consideration from data collection step to classification method, and any artifact will cause inconsistencies among the extracted features.

As noted in [31], training of RBM with binary inputs may be more stable although RBM network was developed for the both cases binary and real values of input units. The purpose of this chapter is to preprocess IVUS signals and binarize extracted patterns for ClassRBM. We propose to binarize the time-series patterns for the classification, the results will be evaluated by the classification performance between before and after binarization of patterns, and compared with the performance of IB-IVUS method for the same task.

3.2 Methodology

As well as the signal preprocessing presented in section 1.3, we propose to apply the quantization of patterns and graph-to-image transformation to receive binary feature vectors corresponding tissues for the classification. Those steps are presented the steps from pattern extract to binary conversion as following:

Pattern Extraction. We assume that the physical properties evaluated over a range of frequencies will pathologically characterize the pixel of tissue. In particular, each pattern of time-series RF signal with the length of l will reflect the characteristic of the middle point of the pattern. The value l=51 is selected for our study.

The extracted patterns containing real-valued radio-frequencies can be used to train ClassRBM. However, under the view that ClassRBM can work better with binary input, that directs us to the work of data binarization. The following steps show the binarization procedures of data.

Pattern Quantization. Pattern quantization is to approximate the real-valued patterns to the integer-valued ones. That work depends on the number of quantization partitions h, called quantization size. Specifically, for a given integer h, the unit interval will be uniformly partitioned into h subintervals in order, then each normalized RF value of patterns falls in one of such subintervals. The order of obtained interval will be its quantized value.

Definitely, the quantization will be unavoidably prone to errors, i.e., the two different patterns of the two classes will be changed to the same after quantization. Theoretically, the bigger quantization size h is the less approximation errors it causes. Of course, as h increases, it requires more input units of classRBM, thus more computation needs. In experiments, to determine h, we carried out a grid search to satisfy that the quantization error is under a predefined error.

Binary Image Conversion. Fig. 3.1 illustrates the process from the time-series pattern in Fig. 3.1(a) to black-white image in Fig. 3.1(c) with the length of pattern l=51 and the height of image h=70. Generally, as a quantized pattern has length of l and quantization size of h, the binary image with size of $h \times l$ where each pixel of the image is set 1 if the quantized pattern graph falls in, and 0 otherwise is the binary image of the given quantized pattern.

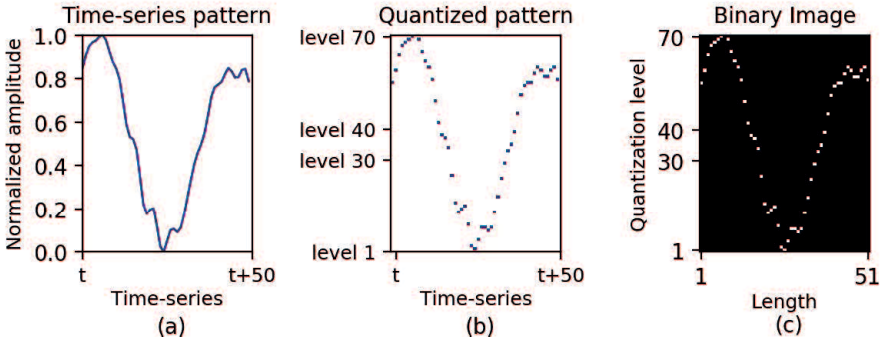

Figure 3.1: Binarization of IVUS featured pattern where picture (a) is a time-series pattern extracted with length of 51 from a time-series point t to $t + 50$ of one IVUS signal, its amplitudes are quantized into 70 levels in picture (b). The corresponding binary image of (b) is shown in picture (c).

3.3 Experiments and results

The experiment dataset includes four coronary artery section of a subject who had a serious coronary heart disease with the occurrence of atherosclerotic plaque in the left circumflex coronary arteries. The medical doctors' examinations showed the atherosclerotic plaque area of those cross sections. Plaque components were identified and classified as three types of plaque tissue: fibrous, fibrofatty and fatty. In particular, the four cross sections with a distance between them is illustrated in Fig. 3.2, and the number of tissues of each cross section is described in Table 3.1.

In data acquisition, a 40-MHz catheter was used. Its rotation speed is 30 revolutions per second and the sampling rate is 210 Hz. In each vessel cross section, 256 A-lines with depth of 1024 are collected. As a result, a 1024×256 matrix of sampled amplitudes corresponds to a vessel cross section.

Fig. 3.3 shows the display in B-mode of the above cross sections, where the colored area is plaque marked by the medical doctors. According to those

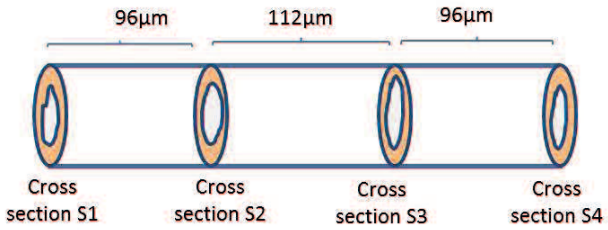

Figure 3.2: Location of interested sections in vessel.

Table 3.1: Number of pixels corresponding to tissues in cross sections

	Fibrous	Fibrofatty	Fatty
Cross section S1	21,288	3,734	1,480
Cross section S2	31,560	4,933	1,338
Cross section S3	42,037	5,016	2,296
Cross section S4	32,176	5,094	894

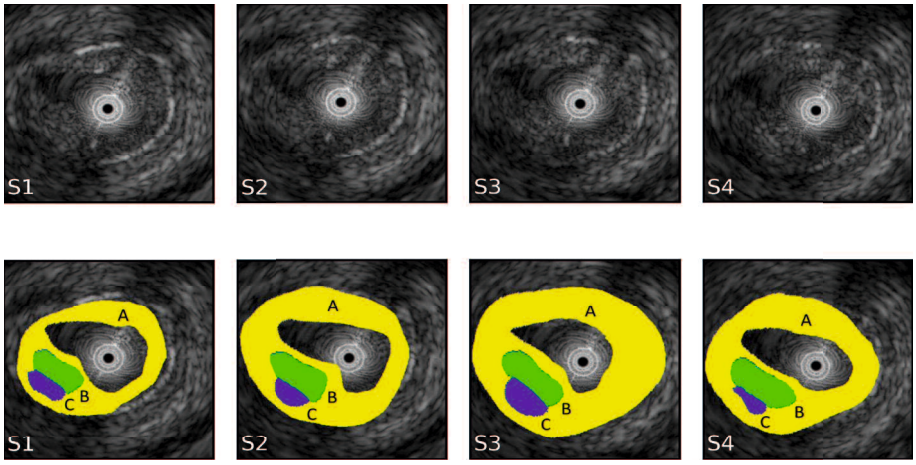

Figure 3.3: B-mode images of four cross sections shown in upper row and their medical doctor's findings correspondingly in the below. A, B and C shades are fibrous, fibrofatty and fatty, respectively.

examinations, the buildup plaque inside the artery of the patient constitutes the prominent fibrous materials (yellow color) as well as fibrofatty (green color) and little core fatty materials (blue).

In experiments, we choose the cross section S2 for training, and tested on the remaining cross sections. To ascertain that the binarization is an advantange, we run ClassRBMs for two cases: the inputs for ClassRBM are the binarization images of the quantized patterns, says B-ClassRBM. And, the other case is non binarization, says N-ClassRBM, i.e., the inputs are patterns of normalized signals. The results are compared each other along with the IB-IVUS method [10, 42].

In training, we used 31,296 fibrous patterns, 4,317 fibrofatty patterns, and 1,177 fatty patterns where the instances close to the boundaries of tissue are not included. Once running ClassRBM by choosing randomly a number of each class, we observed that the number of each class around 6,000 fibrous,

4,000 fibrofatty, and 1,000 fatty is better for both cases: binarization and non binarization.

In setting, we configured the network for the binarization case with 500 hidden units and ran by 30 epochs, while for the non binarization case it contains 500 hidden units and ran by 300 epochs. In both cases, the connection weights were initiated using a uniform distribution with values between -10^{-3} and 10^{-3}. The bias weights in ClassRBM networks were all initiated to zero. The learning rate varied by the number of hidden units H, namely, learning rate was set to $0.1/H$.

For the IB-IVUS method, IB values were calculated by [10]. Here, the IB intervals of three categories obtained from training data are: fibrous ($IB \geq 35.8$), fibrofatty ($28.3 \leq IB < 35.8$) and fatty ($IB < 28.3$).

In evaluation, we compare and contrast methods by two evaluation measures: G-mean and overall accuracy. The predicted values observed by the models are compared to the medical doctor's findings, then G-mean and overall accuracy are calculated. Here, calculating the Recall of each class is based on the rule "one-versus-all". For example, to concern the Recall of *fibrous* we arrange the predicted values and the doctor' findings in a contingency table with the two categories: *fibrous* and *non fibrous*. The Recall of *fibrous* is then defined as Eq. (1.5).

The training and test procedure were repeated 20 times. Each time the training inputs was reselected randomly as aforementioned. The averaged measures are shown in Table 3.2.

It can be seen that the binarization case, B-ClassRBM, mostly received the higher average G-mean values for all these three test cases. B-ClassRBM gives the better results than the two others, whereas the non quantization

Table 3.2: Overall accuracy and G-mean of each test cross section

Test cross section	Method	Accuracy	G-mean
Cross section S1	IB	0.46	0.54
	N-ClassRBM	0.61	0.52
	B-ClassRBM	**0.71**	**0.62**
Cross section S3	IB	0.43	0.54
	N-ClassRBM	0.63	0.58
	B-ClassRBM	**0.65**	**0.67**
Cross section S4	IB	0.42	0.54
	N-ClassRBM	0.60	0.53
	B-ClassRBM	**0.67**	**0.70**

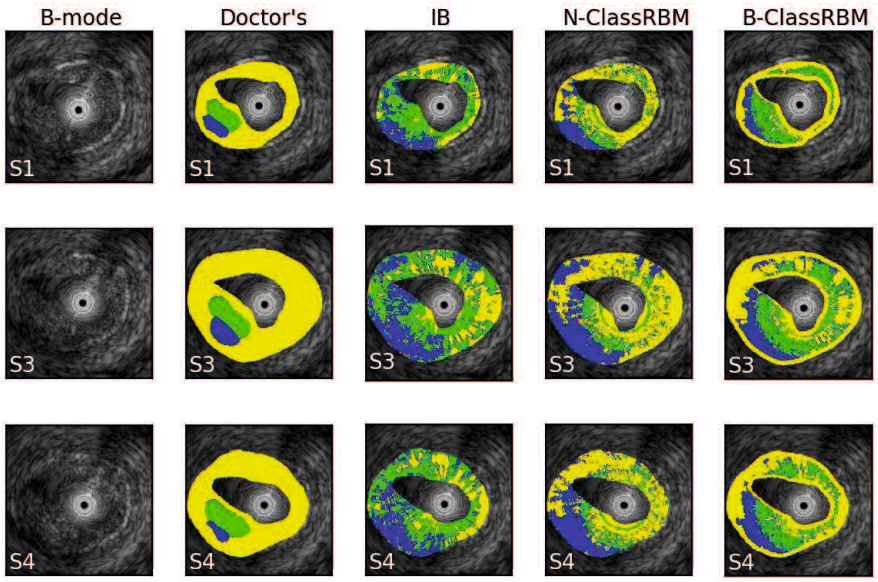

Figure 3.4: Visualization of three test cross sections S1, S3, S4 in the training case of section S2. Column *B-mode* shows B-mode images of test cross sections, column *Doctor's* shows tissues identified by medical doctors, column *IB* shows the classification by IB-IVUS method, columns *N-ClassRBM* and *B-ClassRBM* are the results from non binarization case and binarization case of ClassRBM, respectively.

cases, N-ClassRBM, received the same G-mean as IB method.

On average, the geometric mean of Recalls of all fibrous, fibrofatty and fatty for three test cases are about 0.54, 0.54, and 0.65 for IB, N-ClassRBM and B-ClassRBM, respectively. Taking into account both G-mean and Overall accuracy, it is obvious to ascertain that the binarization cases with ClassRBM can give us not only a better overall accuracy, but also a significantly improved G-mean. The classification capacity of ClassRBM is proved from the results compared to IB-IVUS. Moreover, the accuracy is better when the input data is binarized by the quantization of ultrasound signals.

In regard to visualization, it is clear that not only does B-ClassRBM give a better G-mean but also the enhancement of image is seen as in Fig. 3.4. In addition, tissues identified by B-ClassRBM and N-ClassRBM cases are more compact and close to the medical doctor's findings while the IB method hardly differentiates between fibrous and fibrofatty.

Alternatively, we carried out the same above experiments for the cases that training cross sections were S1, S3 or S4, and the others for test. The test G-means and overall accuracy for those learning cases are listed in Table

Table 3.3: G-means and overall accuracy of learning cases

Train section	Test section	IB		N-ClassRBM		B-ClassRBM	
		Accuracy	**G-mean**	**Accuracy**	**G-mean**	**Accuracy**	**G-mean**
S1							
	S2	0.45	0.65	0.48	0.61	0.60	0.61
	S3	0.40	0.55	0.50	0.62	0.60	0.56
	S4	0.37	0.51	0.43	0.52	0.68	0.65
S3							
	S1	0.45	0.55	0.53	0.63	0.65	0.60
	S2	0.50	0.68	0.55	0.67	0.68	0.67
	S4	0.43	0.58	0.51	0.56	0.64	0.59
S4							
	S1	0.49	0.51	0.55	0.51	0.65	0.62
	S2	0.53	0.60	0.57	0.62	0.69	0.62
	S3	0.50	0.58	0.59	0.60	0.56	0.60

3.3. The results also showed a higher performance of ClassRBM compared to IVUS-IB, although the training sets needed to be chosen with different ratios of classes in each case because of imbalanced data sets.

3.4 Conclusion

In this study, the classification restricted Boltzmann machine was applied to the characterization problem of IVUS tissues. Although, the research dataset is relatively small, the results showed that the classification performance was significantly improved by ClassRBM network compared to the conventional method of Integrated Backscatter (IB). Cross sectional images was also enhanced in visualization.

This study also ascertains that ClassRBM can work more stably with the binary input. In our experience, the quantization of patterns and binarization of input data boosted the learning ability of ClassRBM much better than the real-valued input case. However, when applied the proposed quantization of IVUS patterns, the dataset becomes sparse although this emerging problem has been sovled by the use of L_2-regularization. In addition, the binarization steps of featured patterns gave rise to better tissue classification but, we observed that near field or far field tissues seem to be categorized into same classes as can be seen in Fig. 3.4. Near field artifacts [43] are main factors that cause the miscorrection of data normalization. Those limitations need further considerations.

Although the results showed an improvement by classification restricted

Boltzmann machine, the imbalance of three classes of IVUS data is still the ahead problem to advance the accuracy and visualization quality of IVUS images.

Chapter 4

Two Sub-study Cases about Imbalanced Dataset Learning

4.1 Training restricted Boltzmann machine with synthetic sampling

The objective of this section is to consider sampling techniques to balance the data sets for training of ClassRBM. The results in this section are presented in [44].

4.1.1 Background

The results in chapter 3 showed that RBM could recognize the IVUS tissues better than the conventional method, IB-IVUS. However, the class imbalances had a negative impact on the training of ClassRBM, this is still ahead problem which needs to be tackled.

Medical data analysis is often faced with imbalanced datasets [20, 45]. One of ideas to solve data sets imbalances is to balance the data sets for training. This study uses adaptive synthetic sampling technique (ADASYN) to oversample the minority classes. The balanced training data sets are then used to train classification restricted Boltzmann machine to recognize patterns.

4.1.2 Methodology

Balancing training sets. Imbalanced dataset learning refers to the problem that has an unequal distribution between data classes. This means that

one class outpresents the other classes, i.e., there is a high proportion between classes, for example, 10:1, 100:1, or more severely. The imbalanced data problems often occur in the real-world applications. Moreover, most standard algorithms assume or expect balanced class distributions, that requires us to deal with a compromise of major and minor classes.

The solution to balance the distribution of classes for training is often to oversample the minority sets or undersample the majority sets [20, 46]. Such a well-studied technique is adaptive synthetic sampling (ADASYN) [21]. This method is briefly described in the following:

(i) Define the number of synthetic data examples that need to be generated for the minority class based on the degree of class imbalance.

(ii) Define the number of synthetic data examples the need to be generated for each minority example.

(iii) Generate the synthetic examples corresponding to each minority example with the defined number by linear combination with its random K-nearest neighbors.

Feature extraction. In this study, we use Hamming window with size of 128, then in the time-frequency domain, the patterns of normalized frequencies are extracted corresponding to each point of time. They are then used for the classification.

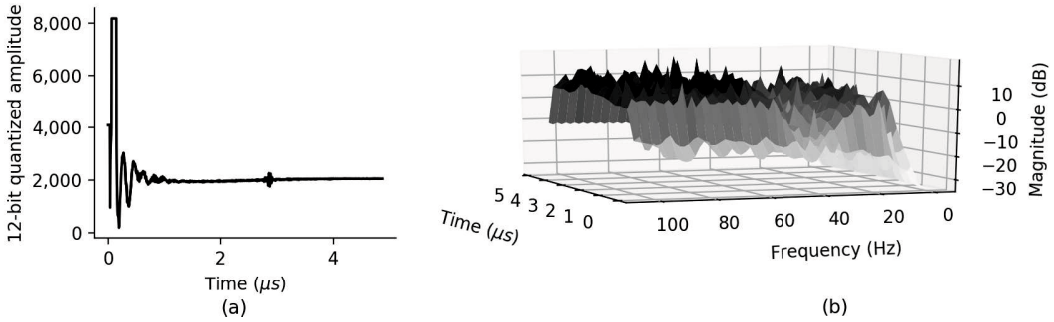

Figure 4.1: Time-frequency transform: (a) is time-series representation of an IVUS signal, and (b) is the time-frequency representation of the signal of (a) by Hamming window.

4.1.3 Experiments and results

Four coronary vessel cross sectional images of left circumflex coronary arteries as in chapter 3 involves this study. In the learning data sets, the plaque area is categorized into fibrous, fibrofatty and fatty tissue classes. Each pixel in a cross sectional image is mapped to the observed tissue by microscope. Table 4.1 shows the class distribution of our four vessel cross sectional images. In the experiments, we selected one cross sectional image for training and the three other ones for test.

To evaluate the classification performance, we use two multiclass evaluation metrics G-mean [18] and MAUC [19]. Shortly speaking, G-mean is the geometrical average of true positive rates, and MAUC is multiclass area under curve. We compare the proposed method with neural networks in the same task.

In settings, the ClassRBM with discriminative training is set up with 500 hidden units, while the neural networks contain 3 hidden layers with the size of 500-300-100. The best case of test is shown in Table 4.2 and Fig. 4.2.

In Table 4.2, the G-means and MAUCs are defined from the total of three test cross sections. Obviously, G-mean of ClassRBM is 0.67 which is higher compared to 0.64 of the neural nets, while there is no significant difference for MAUC.

In the visualizations of cross sections, Fig. 4.2 shows three test cross sections including B-mode images, the medical doctors' findings, the neural nets and ClassRBM. The colored is plaque area. In image displaying, obviously, the ClassRBM shows slightly better performance compared with the neural nets.

Table 4.1: Distribution of fibrous, fibrofatty and fatty class in data sets

Tissue Name	Size	Distribution
Fibrous	127,061	83.7%
Fibrofatty	18,777	12.4%
Fatty	6,008	3.9%

Table 4.2: G-mean and MAUC for ClassRBM and Neural Nets by using ADASYN

Method	G-mean	MAUC
ClassRBM	**0.67**	0.79
Neural Nets	0.64	**0.80**

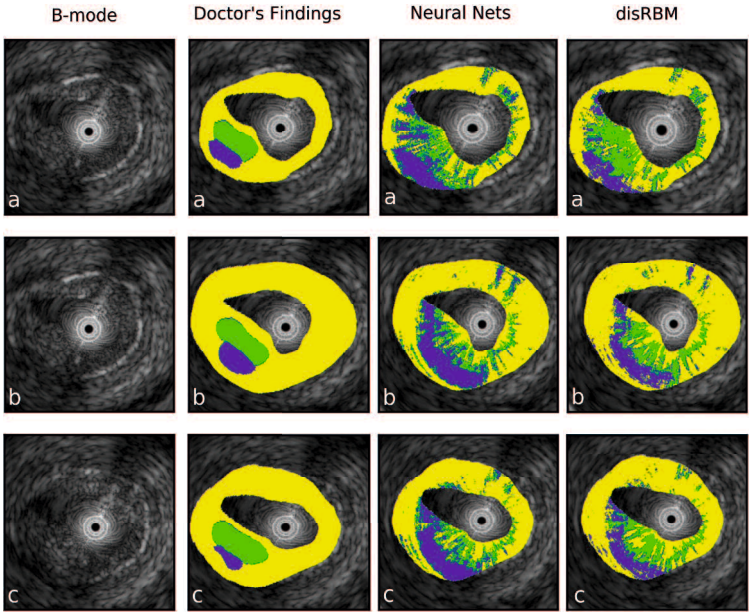

Figure 4.2: Visualization of three test sections denoted a, b, c with their B-mode, doctor's findings, neural nets and ClassRBM display, where yellow is fibrous, blue is fatty and green is fibrofatty.

4.1.4 Conclusion

This study has shown an application of discriminative restricted Boltzmann machine to characterize IVUS tisues with the incorporation of ADASYN technique to balance the training data sets. Although the data sets are relatively small, the experiments showed that ClassRBM could be a considerable classifier compared with neural networks in IVUS tissue characterization.

4.2 Ensembling restricted Boltzmann machines

This section shows an application of multiclass AdaBoost to ensemble ClassRBMs. The results in this section are presented in [47].

4.2.1 Background

In chapter 3, we proposed a technique to binarize IVUS signal patterns. That work boosted the tissue characterization learning compared with training on those extracted patterns. For the binarized instances, generative training model of ClassRBM worked better compared with conventional IB-IVUS method for the same task.

However, existing difficulties need to be addressed those are the imbalances of tissue classes. In our IVUS data sets, tissue components include fatty, fibrofatty and fibrous class, usually, the number of fibrous tissues dominates the two others, specifically around 75% of tissues is fibrous. Section 4.1 has applied the adaptive synthetic sampling (ADASYN) technique which is in terms of balancing training data sets. In this section, we study the capability of ensembling ClassRBMs that aims to tailor all the discrete trained cases instead of single case as previous studies.

Ensembling methods have attracted researchers a lot in recent years as reviewed in [48, 49]. Such effective algorithms are AdaBoost [28], Bagging [26], etc. These algorithms have proved successful applicability in real world. Theoretically, these algorithms were developed independently with classifiers, thus the ensembling of classifiers using these algorithms is practical.

4.2.2 Methodology

IVUS data preprocessing. Frequency patterns extracted from time-frequency transform as in Eq. (1.3). Fig. 4.1 shows the transformation from time-series to time frequency domain, where Hamming window is used.

Multiclass AdaBoost. Zhu et al.[28] developed a very successful technique for boosting the multiclass classification problem. Theoretically, this technique implements an algorithm to combine weak classifiers. We follow the algorithm SAMME of AdaBoost to boost the training of ClassRBM in this study. Specifically, the pseudo-code of SAMME is presented in Algorithm 4.1.

In practice, since the IVUS data sets have class imbalances, training classifiers associated with distribution parameters $w_i's$ tend to be biased towards overfitting of major set or minor set. Thus, we simplify the choice of training samples by randomly choosing, then tailor all the trained classifiers. The schematic diagram for boosting ClassRBMs is described in Fig. 4.3.

4.2.3 Experiments and results

In the experiments, four coronary vessel cross sections involved in this study which positioned the main plaque area. Three of them are mixed and randomly partitioned into training, validation and test sets to study how ClassRBMs can be ensembled. Whereas the number of featured patterns is 125,344 with 4,528 patterns labeled as fatty tissues, 15,043 labeled as fibrofatty tissues, and 105,773 are fibrous tissues. The other section is used to perform visualization.

Algorithm 4.1 SAMME

Input: Training sets X of N examples $(x_1, y_1), \ldots, (x_N, y_N)$ with labels $y_i \in Y = \{1, \ldots, K\}$

Init: Observation weights $w_i = 1/N$ of training sets, $i = 1, 2, \ldots, N$.

for $t = 1$ to M **do**

Training classifier $R^{(t)}$ with respect to weights w_i.

Compute loss:

$$\epsilon^{(t)} = \sum_{i=1}^{N} w_i [c_i \neq R^{(t)}(x_i)] / \sum_{i=1}^{N} w_i.$$

Compute:

$$\alpha^{(k)} = \log \frac{1 - \epsilon^{(k)}}{\epsilon^{(k)}} + log(K - 1).$$

Update :

$$w_i \leftarrow w_i . exp(\alpha^{(k)} [c_i \neq R^{(k)}(x_i)]), \quad i = 1, \ldots, n.$$

Re-normalize w_i

Prediction:

$$C(x) = \arg\max_k \sum_{t=1}^{M} \alpha^{(t)} [R^{(t)}(x) = k].$$

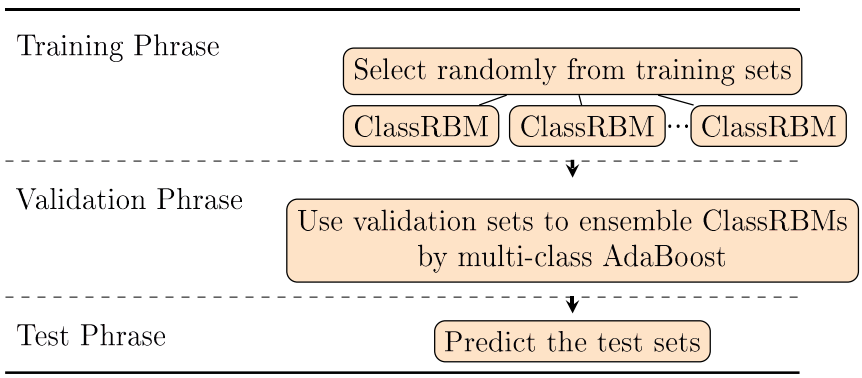

Figure 4.3: Learning schematic diagram of ensembling ClassRBMs.

Two measures overall accuracy and G-mean are used to evaluate the results of our experiments. The results are compared with SVM and Neural Nets for the same tasks. Once training ClassRBMs, the input sets are randomly chosen from training sets. Just after several tests we observed that around 8,000 fibrous patterns with all the fibrofatty and fatty patterns se-

lected for training gave better evaluations.

Table 4.3 shows the results of boosting cases in 120 iterations, where the averaged value of G-means of all individual training cases and the G-mean after boosting are listed to compare. In general, the boosting cases receive slightly better measures compared to the average of individuals except SVM, the boosted G-mean of which is smaller than the averaged one. The G-means of boosting are 54.5, 71.0 and 74.7 for SVM, Neural Nets and ClassRBMs, respectively. Fig. 4.4 shows the trend of G-means by boosting over 120 iterations.

Visualization is another important point we pay attention. The section for visualization check stays independent with learning cases and the visual performance is shown in Fig. 4.5 where the G-means of SVM, Neural Nets and ClassRBMs are 46.9, 57.8 and 61.2, respectively.

Table 4.3: G-means and overall accuracy evaluated in test and visualization sets

	Method	G-mean		Overall accuracy	
		averaged	ensembled	averaged	ensembled
Test sets					
	SVM	60.2	57.1	71.1	72.5
	Neural Nets	73.9	74.5	**74.4**	**75.0**
	ClassRBMs	**74.7**	**74.8**	69.8	70.0
Visualization sets					
	SVM	51.9	49.0	68.3	69.4
	Neural Nets	59.5	59.7	**68.7**	**69.0**
	ClassRBMs	**61.3**	**61.3**	65.2	65.1

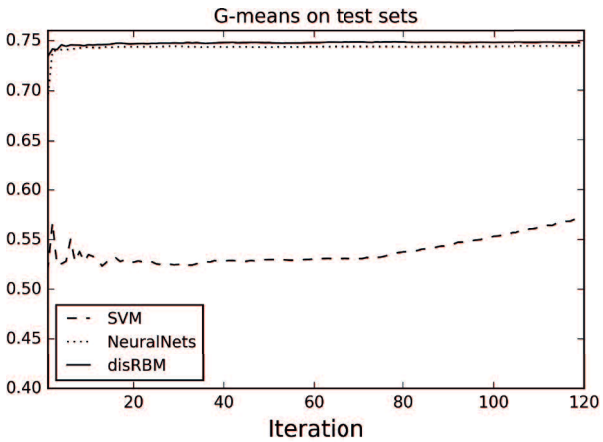

Figure 4.4: G-means of test by multi-class AdaBoost over 120 iterations.

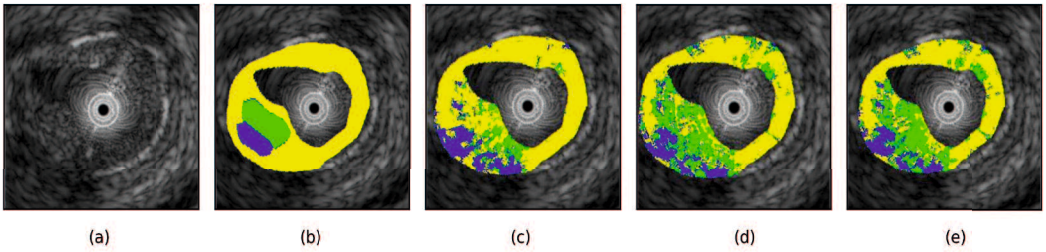

Figure 4.5: Visualization performance where (a) B-mode image, (b) plaque and its components found by medical doctors, (c) SVM, (d) Neural Nets and (e) ClassRBMs. The colored is plaque area where yellow, green and blue are fibrous, fibrofatty and fatty, respectively.

4.2.4 Discussion

This study aimed to ensemble ClassRBMs to characterize IVUS tissues by multi-class AdaBoost. We have shown comparisons how the AdaBoost SAMME algorithm behaved with ClassRBMs, Neural Nets and SVMs. The results proved that ClassRBMs could perform better than the two others. AdaBoost did not crucially improved the accuracy, yet that demonstrated that multi-class AdaBoost could be implemented to work with ClassRBMs on this data. It can be a further consideration to better identify IVUS tissues.

Chapter 5

Misclassification Cost-Sensitive Training of Restricted Boltzmann Machine

This chapter presents an algorithm for training set selection which is sensitive to misclassification of classes. The results in this chapter are presented in [50].

5.1 Background

So far, we have studied the IVUS signals in time series and frequency domains. In chapter 3, we proposed a technique to binarize data for the classification of RBM (classRBM), and chapter 4 showed two sub-studies about tackling the difficulties of IVUS class imbalances are considered. Nevertheless, classRBM performed better as compared with other classifiers such as conventional method integrated backscatter intravascular ultrasound (IB-IVUS), support vector machine and neural network for the same tasks, the difficulties of class imbalances have not been addressed thoroughly as expected, i.e., the output of training classRBM has been significantly affected by the difference of class distributions. In this chapter, we aim to implement an algorithm to solve the class imbalances which is sensitive to the misclassification rate of each individual class. The featured patterns are considered at bit level pertaining to the binary representation of quantized signal amplitudes.

As partially reviewed in Section 1.1, many research fields of machine learning has been applied in IVUS issues, for example, Nair and et al.,[51] proposed autoregressive classification model that used mathematical autore-

gressive model to analyze in frequency domain. Or, using sparse features in [52] or fractal-based features in [53] to characterize tissues in time series domain. Also, wavelet analysis was used in [54] to study IVUS signals and showed that wavelet coefficients could discriminate lipid tissue and others.

Concerning imbalanced datasets, various solutions have proposed involving this kind of issue. In such problem, recognizing major (negative) instances is sometimes not as important as recognizing minor (positive) ones. Besides the techniques of sampling as mentioned in chapter 1 which can balance the training data sets, designing classifier which is sensitive to class distribution is also considerable. Chapter 4 shows the two cases balancing training data sets by sampling; and ensembling classifiers. However, those cases use the traditional algorithm of RBM without any further consideration of the relationship between the training algorithm and its sensitiveness to the training set imbalance degree.

As concluded in chapter 3, ClassRBM worked stably with the binarized IVUS patterns. In addition, the IVUS signals are quantized ones with 12-bit quantization, it means that those quantized signal amplitudes can be displayed in binary series. For that reason, we are interest in the binary level of IVUS data for this study.
In this chapter, the training of ClassRBM which is sensitive to imbalance degree of training sets is studied. The followings show the methodology, experiments and results.

5.2 Methodology

5.2.1 Discriminative restricted Boltzmann machine

Classification restricted Boltzmann machine with discriminative training (DisRBM) is presented in Section 2.2. That learning network is shown as in Fig. 5.1. Each hidden unit h_j connects to visible unit x_i and label unit y_k by connection weights W_{ij} and U_{kj}. If input vector x has class label k, then the corresponding class vector is $y_k = (0, \ldots, \overset{(k)}{1}, \ldots) \in \{0,1\}^K$. Here, K is the number of classes. The objective of discriminative learning is:

$$-\sum_{t=1}^{|X_{sub-train}|} \log p(y_t|\, x_t) \longrightarrow \min\,. \tag{5.1}$$

Here, $|X_{sub-train}|$ is the subset of training sets which is chosen towards balancing training classes. Classification of input vector x with unknown class

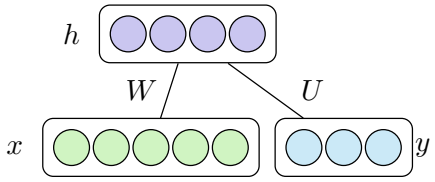

Figure 5.1: Graphical representation of ClassRBM with discriminative training where h is hidden layer, x is input layer , and its class layer y. W and U are connections between hidden units and class units, respectively.

label j in test sets are defined according to the largest output:

$$j = \arg\max_i P(y_i \mid x)\,. \tag{5.2}$$

5.2.2 Pattern Extraction

Fig. 5.2 shows an example of a stained sectional image, its B-mode image and its plaque components from the data sets. And, its acquired IVUS signals are displayed in Fig. 5.3. We extract patches of 5×9 pixels corresponding to 5 adjacent A-lines and 9 time-series points in depth of each A-line in plaque area. The label of a patch is defined by its central point. Each extracted patch is a 5×9 matrix of quantized amplitudes, and these values were already represented in a series of 12 bits by the IVUS transducer quantization. Therefore, amplitude values of patches are represented into binary, hence such a patch responds to a matrix of $5 \times 9 \times 12$ for the classification of DisRBM. In one rough interpretation, this work means that 12 input units of DisRBM are allocated to encode a quantized amplitude of IVUS patches.

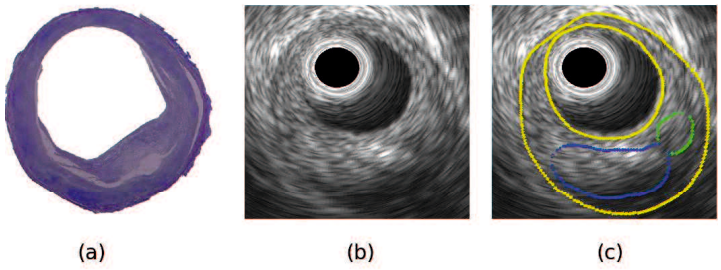

Figure 5.2: The visualization of vessel image. Picture (a) is a cross sectional image of vascular and (b) is the B-mode image of (a). The plaque area is delineated by colored borderlines where fibrofatty is drawn by green line, fatty is drawn by blue line, and the rest area between yellow lines is fibrous.

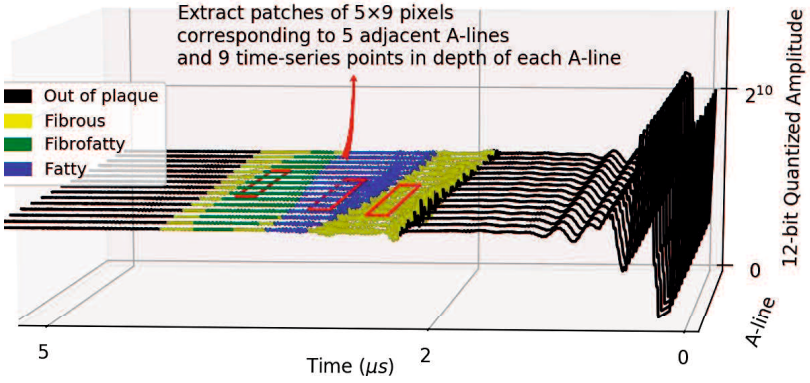

Figure 5.3: Acquired IVUS signals of section in Fig 5.2 is longitudinally displayed. Patches in plaque area are extracted. The colored expresses plaque which is identified by medical experts.

Table 5.1 shows the number of patches extracted from the IVUS data sets, their class and distribution.

5.2.3 Dealing with imbalanced dataset

As the previous discussion, DisRBM is the same as traditional classifiers which seek the overall accuracy. Thus, it tends to identify all the data into the majority class. For the case of class-imbalances, choosing balanced subsets for training is not appropriate because it leads to underfitting of major class. Conversely, the major class will overrepresent the others if all the data sets is used.

To deal with the problem of class imbalances, we propose to use misclassification cost-sensitive training of DisRBM. Specifically, the misclassification cost-sensitive training theme is presented in Algorithm 5.1. The Algorithm 5.1 expresses that the number of training samples is increasingly updated for all classes after each iteration. How many additive training samples are chosen, it depends on the misclassification rate of each class. After

Table 5.1: Distribution of fibrous, fibrofatty and fatty tissues in data sets

Tissue name	Quantity	Distribution
Fibrous	140,576	88.4%
Fibrofatty	14,968	9.4%
Fatty	3,530	2.2%

Algorithm 5.1 Misclassification Cost-Sensitive Training

1: **Input**: Imbalanced training sets X, the number of iterations M.
2: Initialize parameters of classifier R.
3: Choose randomly class-balanced subsets X_{train} from X.
4: **for** $iter = 1$ to M **do**
5: Train R by X_{train} and update the parameters of R.
6: Calculate misclassification rates of classes and the update numbers of classes which are proportional to their misclassification rates.
7: **for** each major class i **do**
8: Resample training sets X_{train} by choosing samples of class i which satisfy that their one-nearest neighbors have the same class as them.

defining the number of training samples, training samples are selected randomly, however in experiments, we only selected such random samples that they are far from the borderlines between classes. In words, every chosen sample must be the same class as its one-nearest neighbors. For the binary vectors, the distance we used is Jaccard metric.

5.3 Experiments

In our IVUS data sets, the plaque area are categorized into fibrous, fibrofatty and fatty tissue classes. Table 5.1 shows the class distribution of our eight vessel cross sections. In the experiments, we used data from five sections for training and the left ones for test.

In settings, the number of hidden units of DisRBM was 200, and learning rate was 10^{-3}. Parameters of DisRBM network were randomly initiated

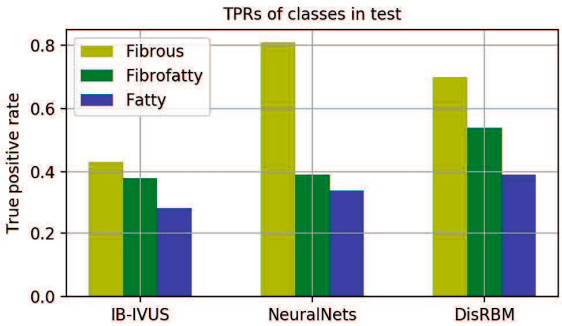

Figure 5.4: Test classification performance by three classifiers IB-IVUS, Neural nets and DisRBM.

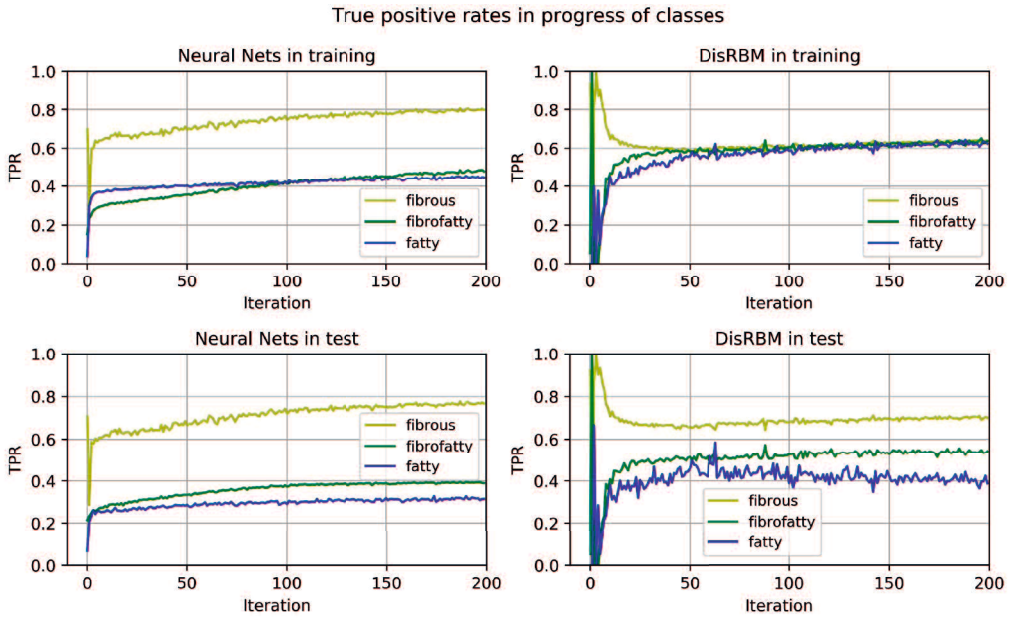

Figure 5.5: Effect of Algorithm 5.1 in training and test of neural network and DisRBM.

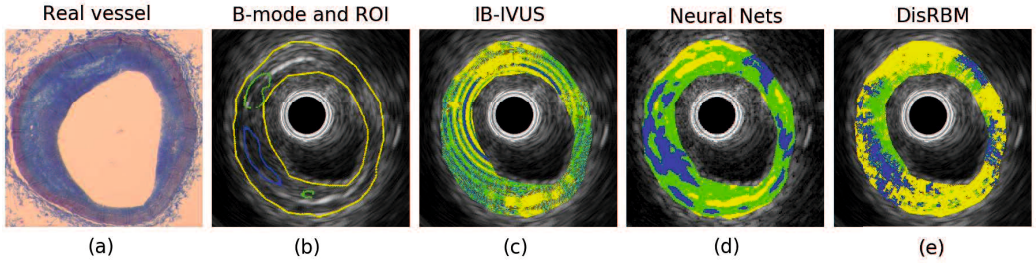

Figure 5.6: Visualization of test classification between IB-IBUS, Neural nets and DisRBM with fibrous, fibrofatty and fatty colored by yellow, green and blue, respectively.

in range $\pm 10^{-5}$. The number of training iteration was set up to 200. We compared ClassRBM with neural network to show how better the misclassification sensitive training algorithm incorporated with ClassRBM or neural network for the same tasks, here neural network has the same network size as ClassRBM. Besides, the classification was evaluated in comparison among IB-IVUS method, neural network and ClassRBM.

We used *true positive rates* (TPRs) for the evaluation. Fig. 5.4 shows the TPRs of test results for IB-IVUS, neural network and ClassRBM. The pro-

posed method is improved as compared with neural network and IB-IVUS. TPRs in Fig. 5.5 displays the progress of TPRs of classes by Algorithm 5.1 between neural network and ClassRBM. In general, Algorithm 5.1 works better with ClassRBM to alleviate the burden of class imbalances.

In visualization, Fig. 5.6 shows one test vessel image with the classification of IB-IVUS, neural network and ClassRBM. Tissues are colored by yellow, green and blue corresponding to fibrous, fibrofatty and fatty. Fig. 5.6(a) shows the stained vessel image, and its B-mode image is constructed as in Fig. 5.6(b) with the region of interest (ROI) drawn by colored lines corresponding to tissue colors. Fig. 5.6(c)-(e) are the classification of IB-IVUS, neural network and ClassRBM correspondingly.

5.4 Conclusion

In this study, we used the discriminative restricted Boltzmann machine to the characterize IVUS signals. We used binary representation of quantized amplitudes of time-series signals, and proposed to use misclassification cost-sensitive training for the classification of ClassRBM. Although, the research data sets are relatively small, the results showed that the proposed method could better characterize as compared with the conventional methods of IB-IVUS and neural network for the same tasks and the same network size.

Chapter 6

Deep Boltzmann Machine

This chapter presents an application of DBM to classify IVUS tissues. Accumulative training of DBM is proposed to deal with IVUS class imbalances. The results in this chapter are presented in [55].

6.1 Background

Using powerful classification frameworks is a trend to handle with large data sets. In medical applications, it has also emerged as an active area of research. This chapter shows an application of deep Boltzmann machines (DBM's) to characterize intravascular ultrasound (IVUS) signals of coronary plaque. An accumulative selection of training sets is introduced, which is sensitive to misclassification rates to deal with class imbalances while the IVUS dataset is concerned at binary level.

Machine learning has become a great concern in medical applications because it provides some powerful learning models for handling big data sets. In the field of machine learning, deep learning [39] has attracted enthusiastic interest in recent years, which is architected by a deep network to handle with large, high dimensional data sets. Restricted Boltzmann machine (RBM) is a good initiation for constructing multiple-layer network [34, 39]. It is a probabilistic model that contains a layer of hidden binary variables connecting to a visible layer of visible variables, and the hidden layer will model the distribution of visible layer [31, 33].

RBM itself can play as a self-contained framework as a classification model [37]. Originally, RBMs were developed using binary stochastic units for both input and hidden layers, and the extension to Gaussian visible inputs were also implemented [31]. The latter case employs data normalization to transform data sets into unit interval or standard normal distribution. In chap-

ters 3,4,5, we used the standalone model of RBM for the classification of IVUS tissues. However, because IVUS signals are affected by near field artifacts, i.e., it results in high amplitudes surrounding transducer [43]. We observed that the data normalization of IVUS signals is significantly affected by those artifacts [40]. In addition, the class imbalances of IVUS training data sets give rise to difficulties of tissue classification.

Pursuing a deep network to learn complicated IVUS data sets better, in this study, we are interested in deep Boltzmann machines (DBM's) [38] as stacked restricted Boltzmann machines (RBM's). We employ a quantization domain to extract binary featured patterns for DBM to avoid near field artifacts by normalization.
The following sections will present about the method, experiments and results in detail.

6.2 Methodology

6.2.1 Deep Boltzmann machine

The DBM network we use in this study is shown in Fig. 6.1 with two hidden layers h^1 and h^2 where x, y are visible and class layers. Architecturally, the DBM includes RBM with (x, h^1) and classification RBM with (h^1, h^2, y). The first RBM transforms data into a low dimensional codes for the classification of the latter one. We call coding phase and classification phase correspondingly.

In coding phase, RBM is trained by stochastic contrastive divergence [31]. In classification phase, we use discriminative training of classification RBM. In prediction, class j of input x is defined by:

$$j = \underset{i}{\operatorname{argmax}}\, P(y_i \mid h^1,\, x)\,. \tag{6.1}$$

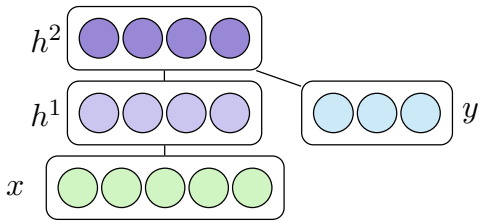

Figure 6.1: Network structure of deep Boltzmann machine with RBM of (x, h^1) and ClassRBM of (h^1, h^2, y) whereas h^1 and h^2 are hidden layers, x and y are input and class layers, respectively.

The readers can refer to [37] for further detail.

6.2.2 Pattern extraction

Fig. 6.2 illustrates the patch extraction where Fig. 6.2 is about a stained vessel section. Its B-mode image is displayed in Fig. 6.2(b). Plaque is drawn as in Fig. 6.2(c) whereas fibrofatty and fatty are enclosed by green and blue lines, respectively. The rest area between yellow lines is fibrous. Time-series signals (A-lines) of vessel section in Fig. 6.2(a) are longitudinally shown in Fig. 6.2(d). We extracted patches of $M \times N$ pixels as red frames in Fig. 6.2(d) whereas yellow, green and blue colored points correspond to the fibrous, fibrofatty and fatty areas in Fig. 6.2(c). Each patch corresponds to an $M \times N$ matrix of quantized amplitudes which were integer-valued ones received from a 12-bit analog-to-digital converter (ADC) of the IVUS transducer. Then, those quantized amplitudes are represented in binary series of 12 bits the

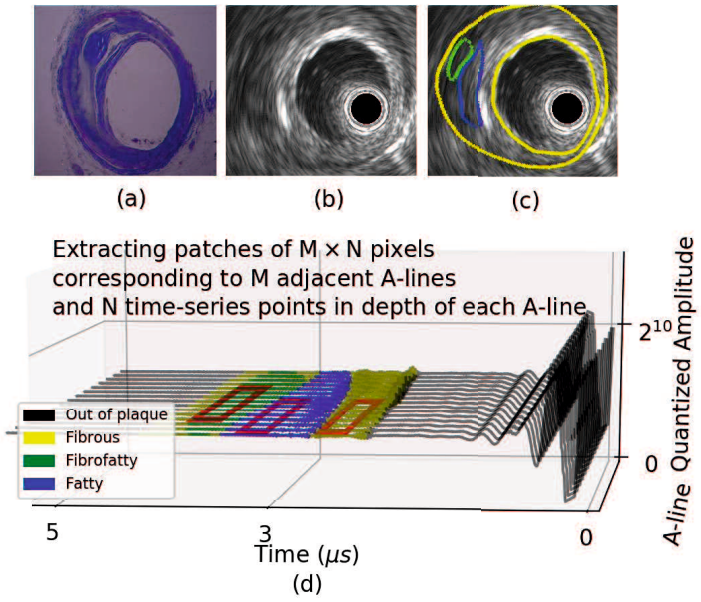

Figure 6.2: Patch extraction from the longitudinal display of time-series IVUS signals where picture (a) is a real vessel and its B-mode display is picture (b). Plaque tissue areas are drawn by borderlines in picture (c) with fatty enclosed by blue line, fibrofatty enclosed by green line, and fibrous in the rest area between yellow lines. The collection of acquired signals from (a) are displayed in (d).

same as the IVUS transducer quantization size. In one rough interpretation, this work is understood that 12 visible units of the DBM are allocated to encode an amplitude.

6.2.3 Dealing with class imbalances

Our IVUS data sets concern three tissue classes fibrous, fibrofatty and fatty. In fact, the distribution of classes is considerably different, and fibrous often outrepresents the rests. Fatty acounts only around 2 percent of the data sets. To deal with the difficulty of class imbalances, in each training epoch of the classification phase of DBM, we reselect the training volume of each class. We follow the idea of the cost-sensitive training scheme in [22] to update the volume of training sets. Shortly speaking, the number of each sub-class chosen for training is accumulated so that it depends on the training cost of previous training step. Here, misclassification rate is defined as training cost. Due to class imbalances, the cost differs between classes so the training sets should be updated in proportions to the misclassification rate of each class.

Specifically, let n_{i*} be the number of samples in class i of training sets, where n_{ij} is the number of i-class samples which are classified in class j. Then, the misclassification rate of class i, say $Miss_i$, is defined by:

$$Miss_i = \frac{\sum_{j \neq i} n_{ij}}{n_{i*}}. \tag{6.2}$$

Now, we add superscript (k) to n_{ij} and $Miss_i$, those are $n_{ij}^{(k)}$, $Miss_i^{(k)}$, to define that they are calculated at the k-th training iteration. Let $n_i^{(k)}$ be the number of i-class training inputs which are chosen at step k. With the above assumption of cost sensitiveness, we define the number of i-class training input samples at step $k+1$ by:

$$n_i^{(k+1)} = n_i^{(k)} + \left[\alpha \times n_{i*} \times \left(Miss_i^{(k)} - \min_j Miss_j^{(k)}\right)\right]. \tag{6.3}$$

Here, [.] is a round function. In the case $n_{i*} < n_i^{(k+1)}$,i.e., the number of i-class samples is defined by Eq. (6.3) is greater than the number of i-class samples in training sets, oversampling is used, otherwise undersampling is used. In the case of oversampling, we use replication. Eq. (6.3) describes the accumulative training volume of each class. The real number α is introduced to control the updated number of training samples. Obviously, if at step k, the misclassification rate is minimized by class i, then the number of i-class samples is unchanged in the next training iteration.

6.3 Experiments and results

The research data sets were provided by the Graduate School of Medicine, Yamaguchi University. Six vessel sections of human left circumflex coronary artery were involved in this study. The ultrasonic observation was carried out using a Galaxy IVUS system (Boston, USA) with a 40 MHz transducer at rotation speed of 30 revs/s, and 256 A-lines were collected in one revolution. The analog signals were sampled at the sampling rate of 210 MHz and quantized by a 12 bit ADC.

We used three coronary sectional images for training and three others for test. Table 6.1 shows the number of each class in datasets. Patches are extracted with five cases of size: 3×5, 5×9, 5×17, 5×25 and 7×17 of pixels, then those patches are represented in 12 bit series as binary stored by the IVUS transducer.

In settings, we set α of Eq. (6.3) equal to 0.1, and the number of iterations equal to 200 in all the cases of classification phase.

Fig. 6.3 shows the classification of test case for the cases of patch sizes

Table 6.1: Number of each tissue class in data sets.

	fibrous	fibrofatty	fatty
Training sets	106,002	12,582	4,585
Test sets	89,440	13,880	3,898

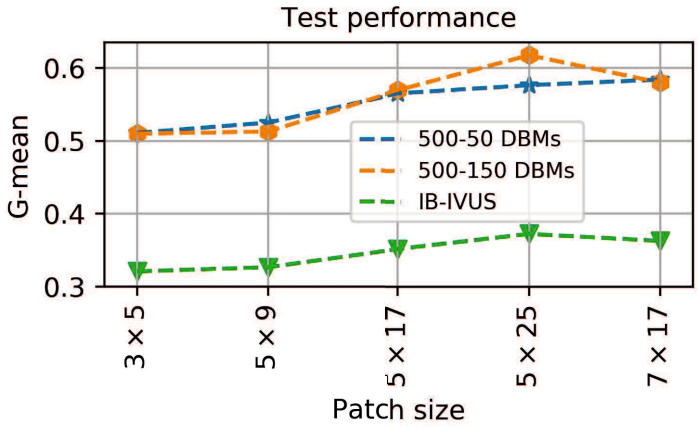

Figure 6.3: Classification of DBM in the cases of patch size.

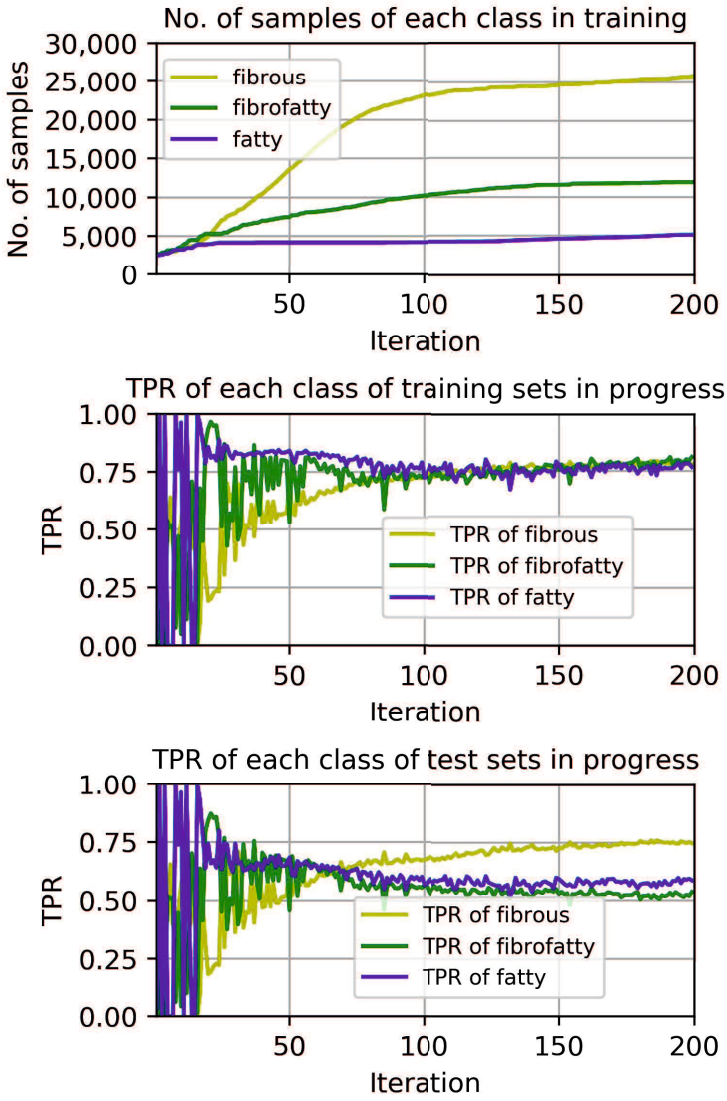

Figure 6.4: Number of samples in each class by Eq. (6.3) and the TPR progress of each class achieved by 500-150 DBM with the patch size case of 5×25.

whereas the DBM has a network size of 500-150, i.e., 500 units of first hidden layer and 150 units of second one. The results are also compared with the performance of IB-IVUS method for the same volumn size. The classification

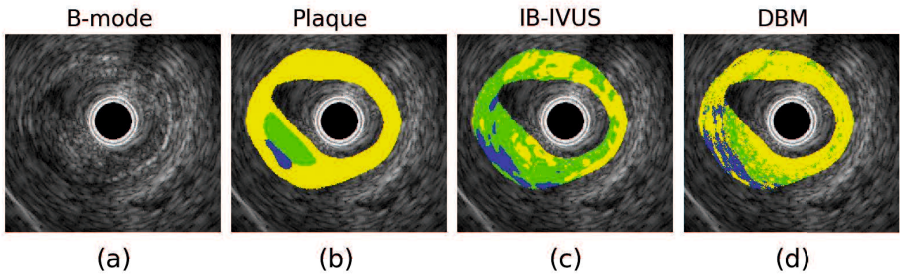

Figure 6.5: Classification performance of one test vessel section by IB-IVUS and DBM with fibrous, fibrofatty and fatty colored by yellow, green and blue, respectively.

performances are assessed by G-mean which is the geometric average of true positive rates (TPR) of all classes. Clearly, the G-means by the proposed method are significantly improved as compared to the conventional method IB-IVUS.

Obviously, the 5×25-size patches are better classified than the others as seen in Fig. 6.3. To show the effect of Eq. (6.3), TPRs of each class are evaluated in each iteration, Fig. 6.4 shows the number of each class defined by Eq. (6.3) and the TPRs corresponding to each iteration step for the patch size case of 5×25 and the 500-150 size of DBM. The trend of TPRs are asymptotically closed, that means that the classification is not significantly affected by the between-class imbalance degree.

Fig. 6.5 shows the classification performance of one test vessel section by IB-IVUS method and DBM with 500-150 of hidden layers, and patch size of 5×25. Fig. 6.5(a) is a B-mode image, Fig. 6.5(b) shows the plaque area drawn by experts, Fig. 6.5(c) and Fig. 6.5(d) show the classification performance of IB-IVUS and DBM, respectively, where yellow, green and blue correspond to fibrous, fibrofatty and fatty, respectively. Obviously, in that IVUS image displays, IB-IVUS recognizes between fibrofatty and fibrous tissues not good as DBM does.

6.4 Conclusion

This study used deep Boltzmann machines to characterize IVUS signals. The bit level of dataset was concerned. We presented an accumulative training selection method to train deep Boltzmann machines that was sensitive to misclassification rates. Although, the research dataset is relatively small, the experiments showed the accumulative effect of the proposed method.

This study proposed a training set selection as in Eq. (6.3), the parameter α was introduced to control the input number of each class. However, it was heuristically defined in the experiments. The optimal value of α should be studied as a future work. In addition, the proposed method has been evaluated by comparison with the conventional method IB-IVUS. The evaluation of the proposed method needs more considerations in comparison with other methods in the literature of IVUS tissue characterization, or other traditional classifiers in the field of machine learning.

Chapter 7

Conclusion and Future Work

Up to now, we have achieved some results of the IVUS tissue classification. The difficulties of IVUS data sets were analyzed, especially the class imbalances between tissues, and the limitation of conventional training algorithm of ClassRBM with imbalanced training sets. This dissertation showed a step-by-step approach to improving the tissue classification performance. In words, the IVUS tissue classification problem was first studied by using the classification model of a standalone RBM without any consideration of class imbalances. The more insights into learning from imbalanced IVUS data sets were studied in next steps. Regarding network structure, from a single hidden layer (RBM) to multiple hidden layers (DBM) were gradually concerned.

The first study in chapter 3 showed a comparison between ClassRBM and the conventional method IB-IVUS. The results proved that, in both interested domains of data representation which are time-series and frequency, ClassRBM could be trained better than IB-IVUS for the same task. More considerably, the proposal of IVUS pattern binarization was advantageous, it could adapt the training stability properties of ClassRBM. That was a noticeable point, thus the quantization of IVUS signals would be taken into account in the next studies.

As well as the consideration of the learning capacity of RBM and DBM in IVUS tissue classification. This dissertation spent much time on tackling the problems of imbalanced dataset learning. Evidently, chapters 4, 5 and 6 mainly solved this problem. Exactly, the proposed training algorithms of ClassRBM and DBM focused on designing a train theme which could force ClassRBM and DBM to be sensitive to between-class imbalance degree. These algorithms well supported the training of ClassRBM and DBM, the more considerations of them should be a future work to improve the IVUS classification.

Although all the evaluations might be inefficient, the achieved results are contributed to a better understanding of the IVUS tissue characterization. In comparison with the conventional methods such as integrated backscatter IVUS and other methods in the literature of machine learning such as support vector machine, neural network, having done work proved a promising prospect of solving the problem by the application of deep learning.

However, the IVUS data sets are small, the above results only shows first steps of using deep learning to characterize IVUS signals. This problem needs further considerations to assess the stability of the proposed method.

References

[1] M. P. Heron, "Deaths: leading causes for 2010," *National Vital Statistics Reports*, Vol.62, No.6, 2013.

[2] A. C. Wal van der and A. E. Becker, "Atherosclerotic plaque rupture-pathologic basis of plaque stability and instability," *Cardiovascular Research*, Vol.41, No.2, pp.334–344, 1999.

[3] S. E. Nissen and P. Yock, "Intravascular ultrasound," *Circulation*, Vol.103, No.4, pp.604–616, 2001.

[4] R. N. Bracewell and R. N. Bracewell, *The Fourier transform and its applications*, McGraw-Hill New York, 1986.

[5] A. Katouzian, S. Sathyanarayana, B. Baseri, E. E. Konofagou and S. G. Carlier, "Challenges in atherosclerotic plaque characterization with intravascular ultrasound (IVUS): from data collection to classification," *IEEE Transactions on Information Technology in Biomedicine*, Vol.12, No.3, pp.315–327, 2008.

[6] F. A. Lupotti, C. L. De Korte, F. Mastik and A. F. Van Der Steen, "Dynamic noise correction for IVUS quantitative volume blood flow: methods and numerical validation," *Ultrasound in Medicine and Biology*, Vol.28, No.8, pp.1053–1060, 2002.

[7] K. Hibi, A. Takagi, X. Zhang, T. J. Teo, H. N. Bonneau, P. G. Yock and P. J. Fitzgerald, "Feasibility of a novel blood noise reduction algorithm to enhance reproducibility of ultra high frequency intravascular ultrasound images," *Circulation*, Vol.102, No.14, pp.1657–1663, 2000.

[8] H. V. Anderson, W. S. Weintraub, M. J. Radford, M. S. Kremers, M. T. Roe, R. E. Shaw, D. M. Pinchotti and J. E. Tcheng, "Standardized cardiovascular data for clinical research, registries, and patient care: a report from the Data Standards Workgroup of the National Cardiovascular Research Infrastructure project," *Journal of the American College of Cardiology*, Vol.61, No.18, pp.1835–1846, 2013.

[9] S. Balocco, C. Gatta, F. Ciompi, et al., "Standardized evaluation methodology and reference database for evaluating IVUS image segmentation," *Computerized Medical Imaging and Graphics*, Vol.38, No.2, pp.70–90, 2014.

[10] F. Ciompi, C. Gatta, O. Pujol, O. Rodriguez-Leor, J. M. Ferre and P. Radeva, "Reconstruction and analysis of intravascular ultrasound sequences," *Recent Advances in Biomedical Signal Processing*, Vol.223, No.243, pp.231–250, 2011.

[11] L. Cohen, *Time-frequency analysis*, Prentice Hall, New York, 1995.

[12] Y. Sun, M. S. Kamel and Y. Wang, "Boosting for learning multiple classes with imbalanced class distribution," *Proceedings of International Conference on Data Mining (ICDM 2006)*, pp.592–602, 2006.

[13] D. D. Lewis and W. A. Gale, "A sequential algorithm for training text classifiers," *Proceedings of the Seventeenth Annual International ACM SIGIR Conference on Research and Development in Information (SIGIR 1994)*, pp.3–12, 1994.

[14] D. M. Powers, "Evaluation: from precision, recall and F-measure to ROC, informedness, markedness and correlation," *Journal of Machine Learning Technologies*, Vol.2, No.1, 2011.

[15] S. Wang and X. Yao, "Multiclass imbalance problems: analysis and potential solutions," *IEEE Transactions on Systems, Man, and Cybernetics, Part B (Cybernetics)*, Vol.42, No.4, pp.1119–1130, 2012.

[16] R. Rifkin and A. Klautau, "In defense of one-vs-all classification," *Journal of Machine Learning Research*, Vol.5, pp.101–141, 2004.

[17] R. C. Bose and C. D. K. Ray, "On a class of error correcting binary group codes," *Information and Control*, Vol.3, No.1, pp.68–79, 1960.

[18] M. Kubat, R. Holte and S. Matwin, "Learning when negative examples abound," *Proceedings of European Conference on Machine Learning (ECML 1997)*, pp.146–153, 1997.

[19] D. J. Hand and R. J. Till, "A simple generalisation of the area under the ROC curve for multiple class classification problems," *Machine Learning*, Vol.45, No.2, pp.171–186, 2001.

[20] H. He and E. A. Garcia, "Learning from imbalanced data," *IEEE Transactions on Knowledge and Data Engineering*, Vol.21, No.9, pp.1263–1284, 2009.

[21] H. He, Y. Bai, E. A. Garcia and S. Li, "ADASYN: Adaptive synthetic sampling approach for imbalanced learning," *Proceedings of the IEEE International Joint Conference on Neural Networks*, pp.1322–1328, 2008.

[22] Z. H. Zhou and X. Y. Liu, "Training cost-sensitive neural networks with methods addressing the class imbalance problem," *IEEE Transactions on Knowledge and Data Engineering*, Vol.18, No.1, pp.63–77, 2006.

[23] W. A. Rivera, "Noise reduction a priori synthetic oversampling for class imbalanced data sets," *Information Sciences*, Vol.408, pp.146–161, 2017.

[24] Z. L. Zhang, X. G. Luo, S. Garcia and F. Herrera, "Cost sensitive back propagation neural networks with binarization techniques in addressing multi-class problems and non-competent classifiers," *Applied Soft Computing*, Vol.56, pp.357–367, 2017.

[25] K. Wickramaratna, M. Chen, S. C. Chen and M. L. Shyu, "Neural network based framework for goal event detection in soccer videos," *Seventh IEEE International Symposium on Multimedia*, pp.8–15, 2005.

[26] L. Breiman, "Bagging predictors," *Machine Learning*, Vol.24, No.2, pp.123–140, 1996.

[27] R. Huang and E. Riloff, "Bootstrapped training of event extraction classifiers," *Proceedings of the 13th Conference of the European Chapter of the Association for Computational Linguistics*, pp.286–295, 2012.

[28] J. Zhu, H. Zou, S. Rosset and T. Hastie, "Multi-class adaboost," *Statistics and Its Interface*, Vol.2, No.3, pp.349–360, 2009.

[29] A. Liaw, M. Wiener, et al., "Classification and regression by randomForest," *R News*, Vol.2, No.3, pp.18–22, 2002.

[30] A. D'Addabbo and R. Maglietta, "Parallel selective sampling method for imbalanced and large data classification," *Pattern Recognition Letters*, Vol.62, pp.61–67, 2015.

[31] G. E. Hinton, "A practical guide to training restricted Boltzmann machines," *Neural Networks: Tricks of the Trade*, pp.599–619, 2012.

[32] G. E. Hinton, "Training products of experts by minimizing contrastive divergence," *Neural Computation*, Vol.14, No.8, pp.1771–1800, 2002.

[33] A. Fischer and C. Igel, "Training restricted Boltzmann machines: an introduction," *Pattern Recognition*, Vol.47, No.1, pp.25–39, 2014.

[34] G. E. Hinton, S. Osindero and Y. W. Teh, "A fast learning algorithm for deep belief nets," *Neural Computation*, Vol.18, No.7, pp.1527–1554, 2006.

[35] J. Ngiam, A. Khosla, M. Kim, J. Nam, H. Lee and A. Y. Ng, "Multimodal deep learning," *Proceedings of the 28th international conference on machine learning (ICML-11)*, pp.689–696, 2011.

[36] N. M. Nasrabadi, "Pattern recognition and machine learning," *Journal of electronic imaging*, Vol.16, No.4, pp.049901, 2007.

[37] H. Larochelle, M. Mandel, R. Pascanu and Y. Bengio, "Learning algorithms for the classification restricted boltzmann machine," *Journal of Machine Learning Research*, Vol.13, No.Mar, pp.643–669, 2012.

[38] R. Salakhutdinov and H. Larochelle, "Efficient learning of deep Boltzmann machines," *Proceedings of the Thirteenth International Conference on Artificial Intelligence and Statistics*, pp.693–700, 2010.

[39] Y. LeCun, Y. Bengio and G. Hinton, "Deep learning," *Nature*, Vol.521, No.7553, pp.436, 2015.

[40] N. T. Kuong, E. Uchino and N. Suetake, "IVUS tissue characterization of coronary plaque by classification restricted Boltzmann machine," *Journal of Advanced Computational Intelligence and Intelligent Informatics*, Vol.21, No.1, pp.67–73, 2017.

[41] M. Kawasaki, H. Takatsu, T. Noda, et al., "In vivo quantitative tissue characterization of human coronary arterial plaques by use of integrated backscatter intravascular ultrasound and comparison with angioscopic findings," *Circulation*, Vol.105, No.21, pp.2487–2492, 2002.

[42] A. Micari, M. Pascotto, A. R. Jayaweera, J. Sklenar, N. C. Goodman and S. Kaul, "Cyclic variation in ultrasonic myocardial integrated backscatter is due to phasic changes in the number of patent myocardial microvessels," *Journal of Ultrasound in Medicine*, Vol.25, No.8, pp.1009–1019, 2006.

[43] G. S. Mintz, S. E. Nissen, W. D. Anderson, et al., "American college of cardiology clinical expert consensus document on standards for acquisition, measurement and reporting of intravascular ultrasound studies (ivus): A report of the american college of cardiology task force on clinical expert consensus documents developed in collaboration with the european society of cardiology endorsed by the society of cardiac angiography and interventions," *Journal of the American College of Cardiology*, Vol.37, No.5, pp.1478–1492, 2001.

[44] N. T. Kuong, E. Uchino and N. Suetake, "Coronary plaque classification with discriminitive restricted Boltzmann machine and adaptive synthetic sampling," *Proceedings of the 19th IEEE Hiroshima Section Student Symposium (HISS 2017)*, pp.260–263, 2017.

[45] L. J. Mena and J. A. Gonzalez, "Machine learning for imbalanced datasets: application in medical diagnostic," *Flairs Conference*, pp.574–579, 2006.

[46] M. Di Martino, A. Fernandez, P. Iturralde and F. Lecumberry, "Novel classifier scheme for imbalanced problems," *Pattern Recognition Letters*, Vol.34, No.10, pp.1146–1151, 2013.

[47] N. T. Kuong, E. Uchino and N. Suetake, "IVUS tissue characterization in time-frequency domain using discriminative restricted Boltzmann machines," *Proceedings of International Workshop on Nonlinear Circuits, Communications and Signal Processing (NCSP 2017)*, pp.405–408, 2017.

[48] T. G. Dietterich et al., "Ensemble methods in machine learning," *Multiple Classifier Systems*, Vol.1857, pp.1–15, 2000.

[49] M. Galar, A. Fernandez, E. Barrenechea, H. Bustince and F. Herrera, "A review on ensembles for the class imbalance problem: bagging-, boosting-, and hybrid-based approaches," *IEEE Transactions on Systems, Man, and Cybernetics, Part C (Applications and Reviews)*, Vol.42, No.4, pp.463–484, 2012.

[50] N. T. Kuong, E. Uchino and N. Suetake, "Recognition of coronary atherosclerotic plaque tissue on intravascular ultrasound images by using misclassification sensitive training of discriminative restricted Boltzmann machine," *Journal of Biomimetics, Biomaterials and Biomedical Engineering*, Accepted, 2018.

[51] A. Nair, B. D. Kuban, E. M. Tuzcu, P. Schoenhagen, S. E. Nissen and D. G. Vince, "Coronary plaque classification with intravascular ultrasound radiofrequency data analysis," *Circulation*, Vol.106, No.17, pp.2200–2206, 2002.

[52] T. Azetsu, E. Uchino, S. Furukawa, N. Suetake, T. Hiro and M. Matsuzaki, "Tissue characterisation of coronary plaques using sparse feature vectors," *Electronics Letters*, Vol.46, No.7, pp.484–486, 2010.

[53] E. Uchino, T. Koga, H. Misawa and N. Suetake, "Tissue characterization of coronary plaque by kNN classifier with fractal-based features of IVUS RF-signal," *Journal of Intelligent Manufacturing*, Vol.25, No.5, pp.973–982, 2014.

[54] A. Murashige, T. Hiro, T. Fujii, K. Imoto, T. Murata, Y. Fukumoto and M. Matsuzaki, "Detection of lipid-laden atherosclerotic plaque by wavelet analysis of radiofrequency intravascular ultrasound signals," *Journal of the American College of Cardiology*, Vol.45, No.12, pp.1954–1960, 2005.

[55] N. T. Kuong, E. Uchino and N. Suetake, "Coronary plaque classification with accumulative training of deep Boltzmann machines," *Innovative Computing, Information and Control Express Letters*, Accepted, 2018.